

Original paper

Titanium-oxide activity during the formation of gold-bearing quartz veins: evidence for closed system behavior

Karel PACÁK, Jiří ZACHARIÁŠ*, Matěj NĚMEC

Institute of Geochemistry, Mineralogy and Mineral Resources, Faculty of Science, Charles University, Czech Republic;
jiri.zacharias@natur.cuni.cz

* Corresponding author



Titanium contents of both vein and magmatic quartz from five Bohemian gold deposits with known P–T history were used to calculate/discuss the titanium oxide activities (a_{TiO_2}) of natural quartz formed in the absence of Ti-buffering phases at 250–550 °C and 0.1–4 kbar.

Data suggest significant variations in a_{TiO_2} during vein quartz formation, due to variation of P, T and growth rate. Negative correlation between a_{TiO_2} and quartz formation temperature was documented for intrusion-related gold deposits, implying quartz precipitation under closed-system conditions (i.e., without substantial equilibration of the ascending fluid with surrounding rocks). We propose a relationship for quantifying disequilibrium quartz formation that can be readily applied to quartz with known P–T history. The relationship was tested on natural samples exhibiting both rapid and slow crystallization. An example of extreme Ti enrichment (up to $\sim 30\times$) in quartz, associated with its rapid growth, is described and discussed.

Keywords: thermobarometry; gold; quartz veins; titanium, Bohemian Massif

Received: 14 April 2020; accepted: 15 February 2022; handling editor: J. Hora

The online version of this article (doi: 10.3190/jgeosci.340) contains supplementary electronic material.

1. Introduction

The titanium content in naturally occurring quartz is dependent on the temperature, pressure and rutile activity during its formation. This relationship is also known as “Titanium in quartz thermobarometry” or, briefly, “TitaniumQ”. Currently, three different experimental calibrations exist for this relationship. The first is represented by the works of Ostapenko et al. (1987), Wark and Watson (2006) and Thomas et al. (2010, 2015), the second by Huang and Audétat (2012), and the third by Zhang et al. (2020). The experiments conducted in these studies were conducted at high temperatures (550–1000 °C), a wide range of pressures (1–20 kbar, with emphasis on 5–10 kbar) and in various media (hydrothermal fluid or rhyolitic melt). These P–T conditions are far more extreme than would be typical for most natural hydrothermal quartz veins (<500 °C, <5 kbar). In addition, the rate of quartz crystallization can also substantially affect the Ti content of quartz grown from hydrothermal fluids (Huang and Audétat 2012). A recent experimental study of Acosta et al. (2020) suggests even additional factors that affect the final concentration of Ti in quartz, specifically the ratio of TiO_2/SiO_2 within the fluid (in contrast to the activity or absolute concentration of the dissolved TiO_2 as proposed by other authors), and surface reaction-controlled kinetic effects.

Finally, ductile or semi-ductile deformation of the quartz is common in many natural quartz vein samples and

may affect their Ti distribution. Several recent experiments focusing on the behavior of Ti during dynamic quartz recrystallization (e.g., Negrini et al. 2014; Nachlas and Hirth 2015; Nachlas et al. 2018) yielded ambiguous results.

Ti-in-quartz thermobarometry has been applied to natural assemblages ranging from magmatic (e.g. Wiebe et al. 2007; Müller et al. 2008; Breiter et al. 2012; Ehrlich et al. 2012; Buthelezi et al. 2017; Nevitt et al. 2017; Ackerson et al. 2018) and metamorphic rocks (e.g. Müller et al. 2007; Spear and Wark 2009; Storm and Spear 2009; Ashley et al. 2013; Cavalcante et al. 2014; Cruz-Urbe et al. 2017) to hydrothermal veins, ore deposits (e.g., Allan and Yardley 2007; Rusk et al. 2008 2011; Barker et al. 2010; Pérez-Alonso et al. 2016; Monnier et al. 2018), mylonites and deformed crustal rocks (e.g. Kohn and Northrup 2009; Grujic et al. 2011; Haertel et al. 2013; Nachlas et al. 2014; Bestmann et al. 2016; Kidder et al. 2018). Finally, a combination of Ti-in-quartz and O-isotope thermometry with diffusion modeling allowed for the estimation of the duration of mineralizing events in porphyry deposits (Cernuschi et al. 2018).

The greatest challenge in employing Ti-in-quartz thermobarometry lies in determining the TiO_2 activity relative to rutile saturation (a_{TiO_2}) during the crystallization/recrystallization of the quartz. In most laboratory experiments, a_{TiO_2} is equal to 1, whereby the presence of rutile in the resulting mineral assemblage is used as an indicator of Ti saturation. Although the presence of rutile

micro inclusions in natural quartz is generally accepted as proof that a_{TiO_2} equals 1, exceptions to this rule seem to exist (e.g., Morgan et al. 2014; Kendrick and Indares 2018). Establishing the correct a_{TiO_2} value in natural samples, notably in quartz veins, is often less straightforward. An excellent, in-depth discussion of a_{TiO_2} evolution/variability during prograde metamorphism of pelitic rock in the absence of rutile was published by Ashley and Law (2015). Such an approach, however, is difficult to apply to hydrothermal quartz veins, which are frequently not in equilibrium with the host rock.

Another challenge lies in the variability of the Ti content on both single grain/crystal and rock/vein scales. Factors operating at the single quartz grain/crystal scale comprise: 1) the temperature (e.g., Ackerson et al. 2018) or pressure of crystallization; 2) disequilibrium quartz growth and/or variable growth rate; 3) the presence of domains with different a_{TiO_2} values (but formed under the same P, T conditions; Kidder et al. 2018); 4) post-crystallization Ti diffusion in high-temperature environments (van den Kerkhof et al. 2004). Factors causing variance on a rock scale are: 5) the presence of multiple quartz generations (formed under different P, T and a_{TiO_2} conditions), or the occurrence of relict quartz (e.g., Kendrick and Indares 2018); 6) insufficient re-equilibration of the relict quartz to

the new P–T conditions (e.g., Ashley et al. 2013; Kendrick and Indares 2018); and 7) recrystallization-driven quartz purification (Simon et al. 2004; Müller et al. 2012).

In general, hydrothermal systems span a continuum between closed and open systems concerning their wall rocks. The vein gangue close to the wall rocks will be formed by precipitation from the fluid driven by the ambient temperature, pressure and their gradients, and internal processes such as boiling, etc. The open system suggests continuous equilibration between the ascending fluid and the surrounding rocks, while the closed system lacks any equilibration. The solubility of rutile in an aqueous fluid decreases with temperature (Antignano and Manning 2008). Therefore a_{TiO_2} will tend to increase in a closed cooling system.

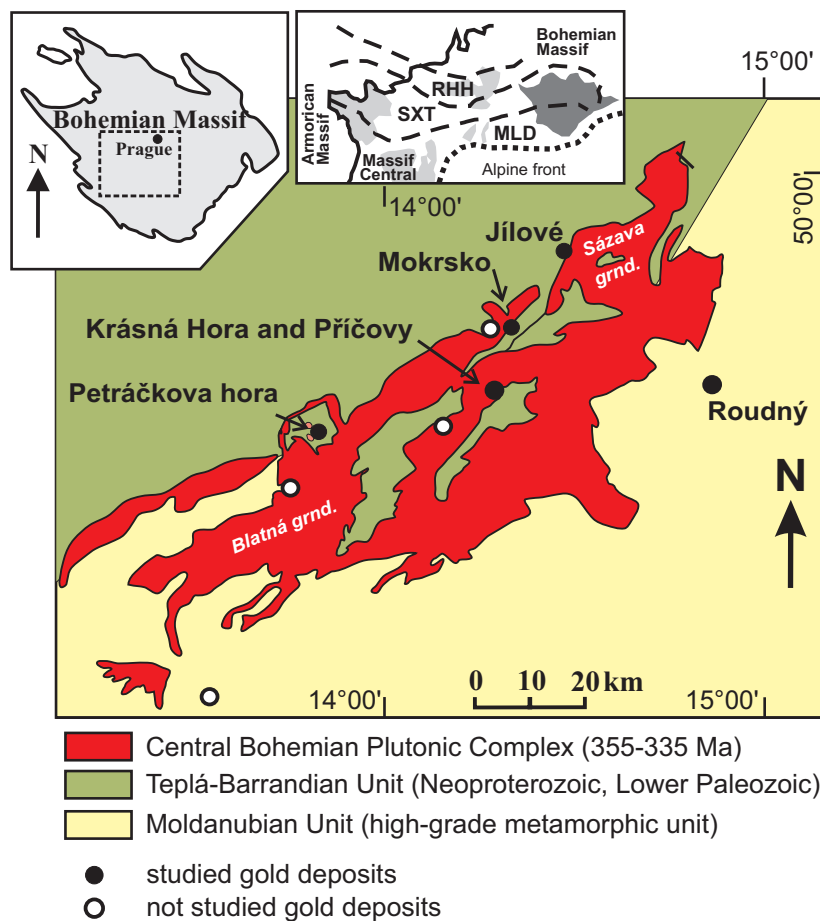
This study provides an empirical test of the variability of a_{TiO_2} and/or TiO_2 oversaturation during the formation of hydrothermal quartz veins under shallow to mid-crustal conditions and in the absence of Ti buffering phases. Thus, this approach is different from most similar empirical studies that tended instead to focus on P or T determination, while the value of a_{TiO_2} was assumed to be known and generally fixed over a wide range of P and T.

Because our hydrothermal quartz crystallized at pressures of 0.1–4 kbar, we decided to use the Ti-in-quartz calibration of Thomas et al. (2010), which is best suited to the P–T range and crystallization medium of our samples; use of the other extant thermobarometer formulations would have required extrapolation far beyond the range of intensive variables for which they were calibrated. This calibration was applied to our recently published quartz trace-element data (Pacák et al. 2019), representing successive quartz vein generations from several Bohemian gold deposits. As some of our calculations resulted in $a_{\text{TiO}_2} > 1$, we introduced a new parameter (X^*) that allows simple expression of the deviation of the measured Ti content in the quartz with respect to its equilibrium content, for the given P and T values.

2. Regional geology and metallogeny

Numerous hydrothermal vein-type gold deposits are located along the north-

Fig. 1 Studied gold deposits and schematic geological map of the Central Bohemian Plutonic Complex (CBPC) and its surroundings.



Tab. 1 A brief overview of the studied deposits and distinguished quartz types (for the P–T conditions of quartz formation, see Tab. 2 or Fig. 3).

Dep.	Subtype	Gold resources (host rock)	Vein/quartz types (general characterization and abundance)	References
Mokrosko-West	high-fineness Au (IRG/ORG)	~90 t @ 1.8 g/t Au granodiorite	Q _{grnd} – magmatic quartz of granodiorite groundmass Q _{peg} – quartz from a pegmatite body about 100 m far from the granodiorite Q ₀ – minor, pre-ore barren subhorizontal veins Q ₁ – early ore veins (subvertical, more than 20 cm thick) Q _{1,2} – abundant, main ore veins, subvertical, up to 10 cm thick (may represent Q ₁ or Q ₂ types, or a transition between them) Q ₂ – very abundant, main ore veins, subvertical sheeted densely spaced, < 5 mm thick Q ₃ – sparse, moderately dipping, post-Q ₂ veins	Morávek et al. (1989) Boiron et al. (2001) Zachariáš et al. (2014) Zachariáš (2016) Wertich et al. (2018)
Petráčkova hora	high-fineness Au (IRG)	~33t @ 1.1 g/t Au or ~7t @ 2.0 g/t Au granodiorite	Q _{grnd} – magmatic quartz of granodiorite groundmass Q _{apl} – quartz lens (5 x 10 cm) enclosed in aplite dyke hosted by granodiorite Q ₁ – sparse, early ore veins with K-feldspar alteration rim Q ₂ – most abundant, main ore veins, no alteration, up to 50 g/t Au Q _{2,3} – minor, no alteration, abundant scheelite Q ₄ – abundant, later phase of ore veining, no alteration, < 10 g/t Au Q ₅ – minor, late veins (traces of Au only), subhorizontal	Zachariáš et al. (2001)
Jílové	high-fin. Au (ORG)	~10 t @ 6 g/t Au metavolcanites (& granodiorite porphyry)	Q ₁ – main gold-bearing veins Q ₂ – rare vein type, molybdenite-bearing Q ₃ – late quartz filling fractures in Q ₁ , associated with native arsenic and base-metal sulphides/sulphosalts	Morávek (1971), Zachariáš et al. (2013)
Roudný	low-fin. Au–Ag (ORG)	~6 t @ 10 g/t Au altered gneiss	Q ₁ – sparse early quartz veins (Q ₁) with tourmaline (of unclear relation to ore-mineralization, may represent late-metamorphic veins) Q ₂ – unambiguous ore-related veins, abundant As-bearing pyrite and arsenopyrite (both contain invisible gold) Q ₃ – late quartz (Q ₃) fill (early phase of formation of Q ₃ is seems associated with deposition of macroscopic gold)	Zachariáš et al. (2004, 2009); Zachariáš and Hübst (2012)
Krásná Hora	high-fin. Sb–Au (ORG)	~1.5 t @ 3–5 g/t Au Lamprophyre dikes within granodiorite	Q ₁ – early veins with sparse arsenopyrite (most of them are Au-barren) Q ₂ – main ore veins associated with deposition of stibnite (coarse-grained) Q ₃ – late ore quartz (Q ₃), fills in fractures in Q ₂ or Q ₁ , predates/accompany gold	Němec and Zachariáš (2018), Zachariáš and Němec (2017)
Příčovy	high-fin. Sb–Au (ORG)	~0.5 t @ 9.4 g/t Au Lamprophyre and granod. porphyry dikes within granodiorite	Q ₁ – not present at the deposit Q _{2a} – fine-grained quartz intergrown with Sb-phases (stibnite and zinkenite) Q _{2b} – coarse-grained quartz intergrown with Sb-phases (stibnite and zinkenite) Q _{2c} – coarse-grained quartz intergrown with Al-phases (dickite/kaolinite)	Němec and Zachariáš (2018)

western margin of the Central Bohemian Plutonic Complex (CBPC; Fig. 1). This zone also represents a boundary between the low-metamorphic-grade Teplá-Barrandian (TBU) and high-metamorphic-grade Moldanubian units. Formation of the gold deposits (e.g., 348–338 Ma, Zachariáš and Stein 2001; Zachariáš et al. 2013, 2014; Ackerman et al. 2017) broadly overlaps with the intrusive activity of the CBPC (355–335 Ma; Janoušek and Gerdes 2003; Janoušek et al. 2004, 2010), as well as with the regional metamorphism in the Moldanubian unit ~355 and 335 Ma (e.g., O'Brien and Rötzler 2003).

The Central Bohemian Plutonic Complex (3200 km²) consists of five to seven magmatic suites (Holub et al. 1997), evolving from the older calc-alkaline (I-type) to potassium-rich calc-alkaline suites (I/S and S types) and

to the younger ultrapotassic suite (Tábor pluton). Schulmann et al. (2009) interpreted the CBPC as an Andean-type magmatic arc associated with the Saxothuringian unit/plate subduction beneath the Teplá-Barrandian and Moldanubian units.

The Teplá-Barrandian unit (Fig. 1) represents part of the Avalonian–Cadomian belt that developed along the active northern margin of Gondwana during the late Neoproterozoic (~750 to 540 Ma; e.g., Linnemann et al. 2008). The Neoproterozoic rocks (volcanic, volcano-sedimentary and flysh-like sequences) form several juxtaposed, NE–SW trending, allochthonous belts separated by shear zones. These belts have been interpreted as remnants of an oceanic crust, several accretionary wedges and a single volcanic arc (Hajná et al. 2011). The

Tab. 2 Summary descriptive statistics of Ti contents in the studied quartz types/veins (based on the dataset of Pacák et al. 2019). For the definition of X^* , see the Discussion. MAD = median absolute deviation of the median; IQR = interquartile range (difference between 75th and 25th percentiles)

Deposit	Dep. type	Quartz type	T (°C)	P (kbar)	N (data)	Median (ppm)	Mean (ppm)	Min (ppm)	Max (ppm)	St. Dev. (ppm)	IQR (ppm)	MAD (ppm)	X*(TH10) (ratio)
Petráčkova hora	IRG	Q _{grnd}	650	3.5	6	74.6	71.0	53.7	88.8	14.3	24.9	9.5	0.49
Petráčkova hora	IRG	Q _{apl}	600	3.0	8	77.3	76.8	52.2	90.5	12.6	16.2	8.0	0.73
Petráčkova hora	IRG	Q ₁	510	2.5	9	14.6	14.7	11.7	18.3	2.4	5.2	2.5	0.35
Petráčkova hora	IRG	Q ₂	470	2.0	11	20.0	18.9	11.1	25.5	5.1	10.3	4.2	0.71
Petráčkova hora	IRG	Q ₂₋₃	470	2.0	11	28.0	29.5	20.8	41.8	5.5	6.1	2.1	0.99
Petráčkova hora	IRG	Q ₄	450	2.0	21	15.6	16.6	11.0	26.2	4.4	4.2	1.9	0.74
Petráčkova hora	IRG	Q ₅	450	1.7	9	31.1	31.3	21.7	41.5	7.3	12.3	6.3	1.34
Mokrsko-West	IRG	Q _{grnd}	680	4.0	17	47.5	56.8	38.0	84.7	16.2	30.2	5.5	0.26
Mokrsko-West	IRG	Q _{peg}	600	4.0	17	11.3	11.5	5.1	17.9	3.1	4.4	2.4	0.14
Mokrsko-West	IRG	Q ₀	550	4.0	17	21.5	21.4	18.1	26.0	2.7	4.6	2.6	0.46
Mokrsko-West	IRG	Q ₁	500	3.2	116	9.4	10.0	3.8	20.4	3.5	4.5	2.3	0.31
Mokrsko-West	IRG	Q ₁₋₂	460	3.0	171	10.3	13.2	3.4	35.0	7.8	11.7	3.8	0.56
Mokrsko-West	IRG	Q ₂	450	3.0	154	8.5	8.8	2.0	17.0	2.9	3.7	1.8	0.53
Mokrsko-West	IRG	Q ₃	400	2.8	11	5.7	5.9	4.0	7.9	1.2	1.7	0.9	0.76
Jílové	ORG	Q _{1a}	350	2.0	5	1.8	1.8	1.6	2.3	0.3	0.3	0.2	0.48
Jílové	ORG	Q _{1b}	350	2.0	6	1.7	1.9	1.7	2.5	0.4	0.5	0.1	0.46
Jílové	ORG	Q ₂	380	2.0	7	4.9	4.6	4.0	5.2	0.6	1.1	0.3	0.73
Jílové	ORG	Q ₃	250	0.1	4	2.2	2.1	2.0	2.5	0.3	0.4	0.2	2.66
Roudný	ORG	Q ₁	550	2.5	13	30.9	31.6	25.2	39.8	4.4	6.4	3.0	0.45
Roudný	ORG	Q ₁₋₂	450	1.75	10	9.1	9.0	7.6	10.4	0.8	0.9	0.5	0.4
Roudný	ORG	Q ₂	355	0.45	25	2.4	2.6	1.6	4.8	0.9	1.0	0.5	0.34
Roudný	ORG	Q ₃	320	0.10	12	3.0	2.6	1.7	3.2	0.7	0.9	0.3	0.75
Krásná Hora	ORG	Q ₁	450	2.5	25	18.0	23.2	11.7	53.5	10.2	12.0	4.2	0.98
Krásná Hora	ORG	Q ₂	350	1.0	86	2.9	3.5	1.8	9.9	1.6	1.8	0.7	0.54
Příčovy	ORG	Q _{2a}	300	1.0	5	24.8	25.0	19.9	31.2	4.4	4.7	2.7	13.43
Příčovy	ORG	Q _{2b}	300	1.0	4	1.1	1.1	0.8	1.4	0.3	0.5	0.3	0.60
Příčovy	ORG	Q _{2c}	300	1.0	31	1.6	2.8	0.9	15.6	3.2	2.9	0.8	0.87

volcano-sedimentary Jílové Belt (which hosts some of the studied gold deposits) is the easternmost part of the TBU.

The Moldanubian unit (Fig. 1) comprises the metamorphosed pre-Variscan (Precambrian/Early Paleozoic) crust and the Variscan granitoids (e.g., Dallmeyer et al. 1995). The unit is further subdivided into the Gföhl and Drosendorf units. The former underwent Variscan HP-HT metamorphism, followed by subsequent rapid exhumation and re-equilibration under mid-crustal conditions. The latter only underwent mid-crustal LP-HT metamorphism (at about 335 Ma; e.g., O'Brien 2000). The main rock types forming the Gföhl unit are leucocratic granulites and migmatitic orthogneisses, while the Drosendorf unit is dominated by paragneiss, orthogneiss, marble, quartzite and amphibolite rocks.

The studied gold deposits can be classified as orogenic gold (ORG) or as intrusion-related gold (IRG) deposits, with some intermediate types (IRG/ORG). They differ in gold fineness, gold-associated metals (Au, Ag–Au, and Sb–Au) and ore mineralogy. The deposits were formed in similar to identical geological settings, over a relatively brief period of time (350–335 Ma; Zachariáš and Stein 2001; Zachariáš et al. 2013, 2014; Ackerman et al. 2017); only the Roudný deposit is probably younger

(~300 Ma). Most of them are hosted by granitoids of the CBPC (Mokrsko-West, Petráčkova hora, Krásná Hora and Příčovy deposits), while the Jílové deposit occurs in the TBU, however close to its contact with the CBPC. The Roudný deposit is hosted by the Moldanubian Unit and lacks any spatial/temporal relation to the CBPC. Table 1 gives a brief summary of the individual deposits and distinguished quartz types, while the P–T conditions of quartz formation are summarized in Tab. 2. Electronic Annex (EA-1) provides a somewhat more detailed description of the deposits and quartz types.

3. Methods

The data used in this study (Tab. 2, Fig. 2a) represent part of the dataset published by Pacák et al. (2019). However, the data themselves have not yet been interpreted/discussed in terms of Ti-in-quartz thermobarometry. The last two data rows in the Tab. 2 (Příčovy deposit, samples P_{2b}, P_{2c}) were originally excluded from Pacák et al. (2019) because the quartz was finely intergrown with zinkenite (Pb₉Sb₂₂S₄₂; sample P_{2b}) and dickite/kalinite (Al₂Si₂O₅(OH)₄; sample P_{2c}). As ²⁹Si was used as

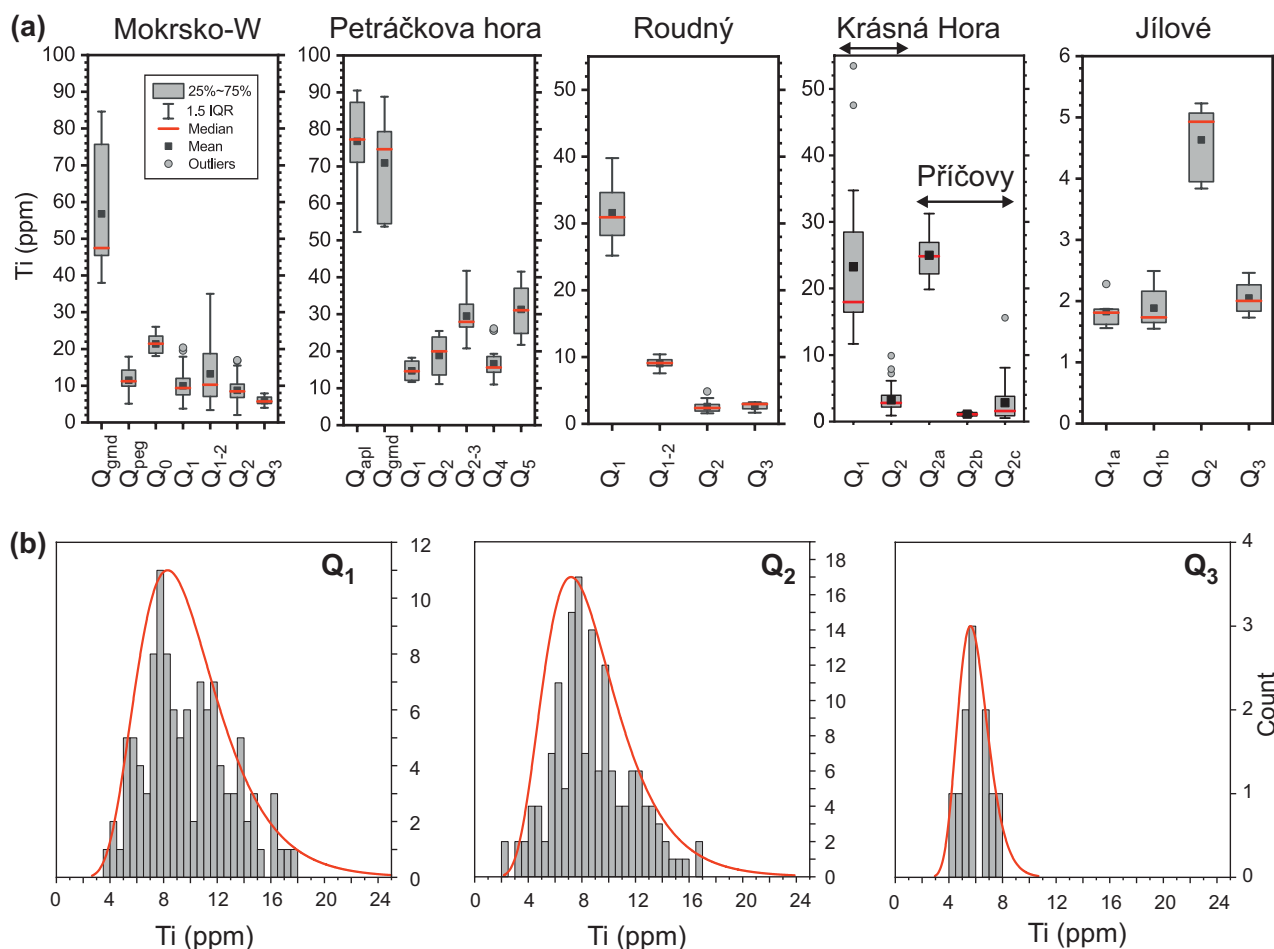


Fig. 2 Distribution of Ti abundances: **a** – at the studied deposits in the identified vein types based on data published by Pacák et al. (2019) and summarized in Tab. 2 herein; **b** – in the Q₁, Q₂ and Q₃ quartz veins at the Mokrsko-West deposit (an IRG deposit). The lognormal distribution curve (thick red line) is shown for comparison.

an internal standard and SiO₂ content was normalized to 99.95 wt. %, the presence of zinkenite does not affect the calculated Ti content of quartz (P_{2b} sample). On the other hand, submicroscopic inclusions of dickite/kaolinite dilute the ²⁹Si signal and the calculated Ti content of P_{2c} sample is slightly lower than it would correspond to “pure” quartz. As the two samples demonstrate the effect of the quartz growth rate on its Ti content, we decided to include them in the current dataset.

The Ti abundances were established by the LA-ICP-MS technique at the Institute of Geochemistry, Mineralogy and Natural Resources at the Faculty of Science, Charles University, using the New Wave UP “213” laser ablation system (Nd:YAG 213 nm) coupled with the Thermo Scientific “iCAP Q” mass spectrometer. Data were acquired as ⁴⁹Ti isotope using ablation line 1 mm in length, 80 μm in width and about 40 μm in depth. The external calibration was performed using the Standard Reference Material NIST 612 and 610 (National Institute of Standards and Technology, USA) with an internal standardization using ²⁹Si by normalizing to 99.95 wt. %

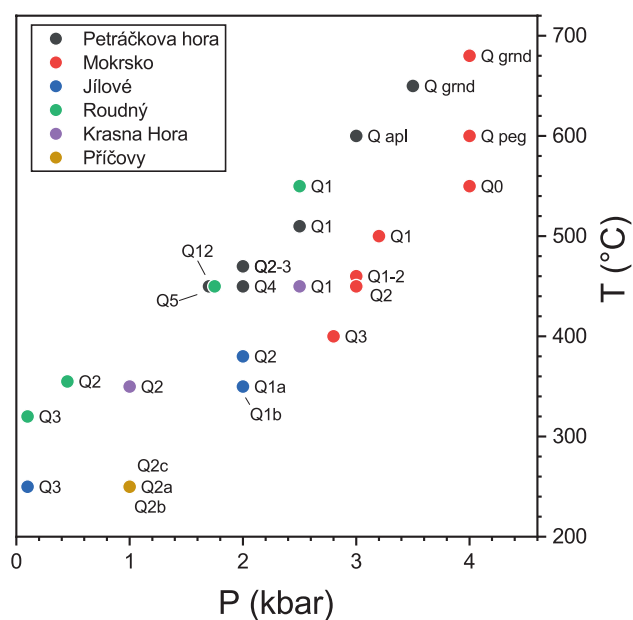


Fig. 3 Overview of the P–T condition of formation of the studied quartz vein types.

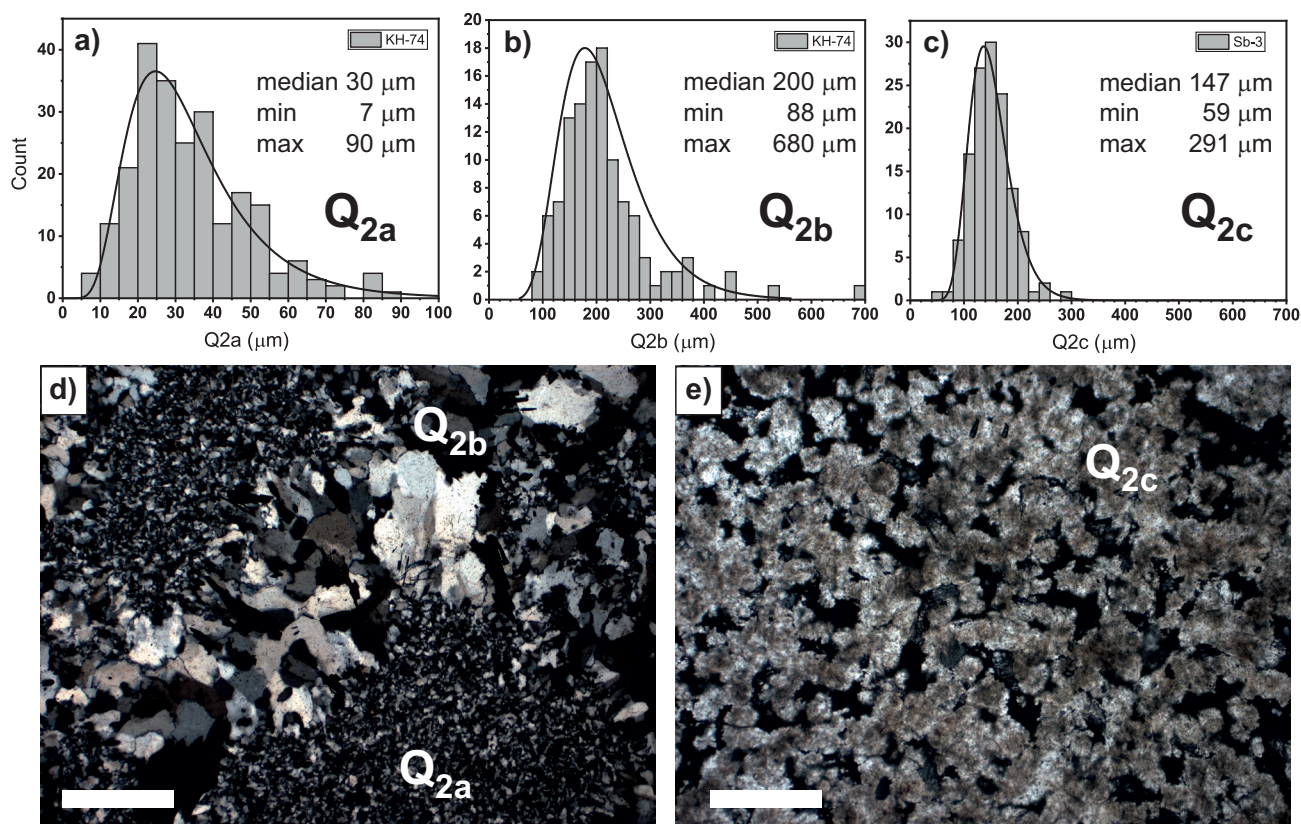


Fig. 4 Grain-size characterization of quartz types from the Příčovy Sb–Au deposit: **a** – grain size distribution of Q_{2a} quartz (~25 ppm Ti); **b** – Q_{2b} quartz (~1.1 ppm Ti); **c** – Q_{2c} quartz (~1.6 ppm Ti). Lognormal distribution curve is shown for comparison. Note that Q_{2a} and Q_{2b} quartz types come from the same vein (sample KH-74). **d–e** – Optical microscope photographs documenting grain-size differences and vein quartz texture (crossed-nicols, scale bar is 0.5 mm).

SiO_2 . Mean detection limit is 1.1 ppm Ti ($n = 1049$). For a detailed description of the analytical settings, data acquisition and processing, see Pacák et al. (2019).

The median values of the Ti abundances (Tab. 2) are used through this paper for all the calculations of a_{TiO_2} during the formation of quartz vein. We believe they best represent the Ti content of the most abundant quartz grain population of a hydrothermal quartz gangue sample.

The P–T conditions (Tab. 2 and Fig. 3) of formation of the individual vein types (or quartz generations) are largely based on a combination of O-isotope thermometry (quartz–scheelite, quartz–hornblende and K-feldspar–hornblende pairs), fluid inclusion isochores and arsenopyrite thermometry, as reported in the original papers summarized in Tab. 1.

4. Results

4.1. Brief description of studied quartz veins and quartz gangue

The studied samples represent typical massive quartz gangue from several ORG and IRG Bohemian gold deposits formed over a wide range of P–T conditions

(Fig. 3, Tab. 2). Classification of quartz veins (Q_1 , Q_2 , etc.) is based on macrostructural criteria and crosscutting relationships on a deposit scale. Up to eight samples of each vein type were analyzed at some deposits (e.g., Mokrsko). These can be easily recognized by a large amount of data (Tab. 2). If a particular vein type exhibited marked textural (e.g., grain size) or paragenetic variability, quartz was categorized into subtypes. For example, three subtypes of Q_2 quartz were distinguished at the Příčovy deposit: the Q_{2a} quartz, although α -quartz, is extremely fine-grained (median 30 μm ; Fig. 4a), compared to the Q_{2b} (median 200 μm ; Fig. 4b), and Q_{2c} (median 147 μm ; Figs. 4c and 4e) quartz subtypes.

Generally, anhedral quartz grains of variable size predominated in the quartz gangue, while euhedral crystals were almost absent. Most samples showed evidence of low to moderate ductile deformation, such as undulatory extinction, the presence of subgrains, or grain-boundary migration. There were practically no strain-free samples.

A single quartz generation predominated in the individual vein samples and we tried to avoid analysis of mixed quartz generations (e.g., microveinlets with younger quartz). The homogeneity of the quartz gangue was further checked by optical cathodoluminescence. No

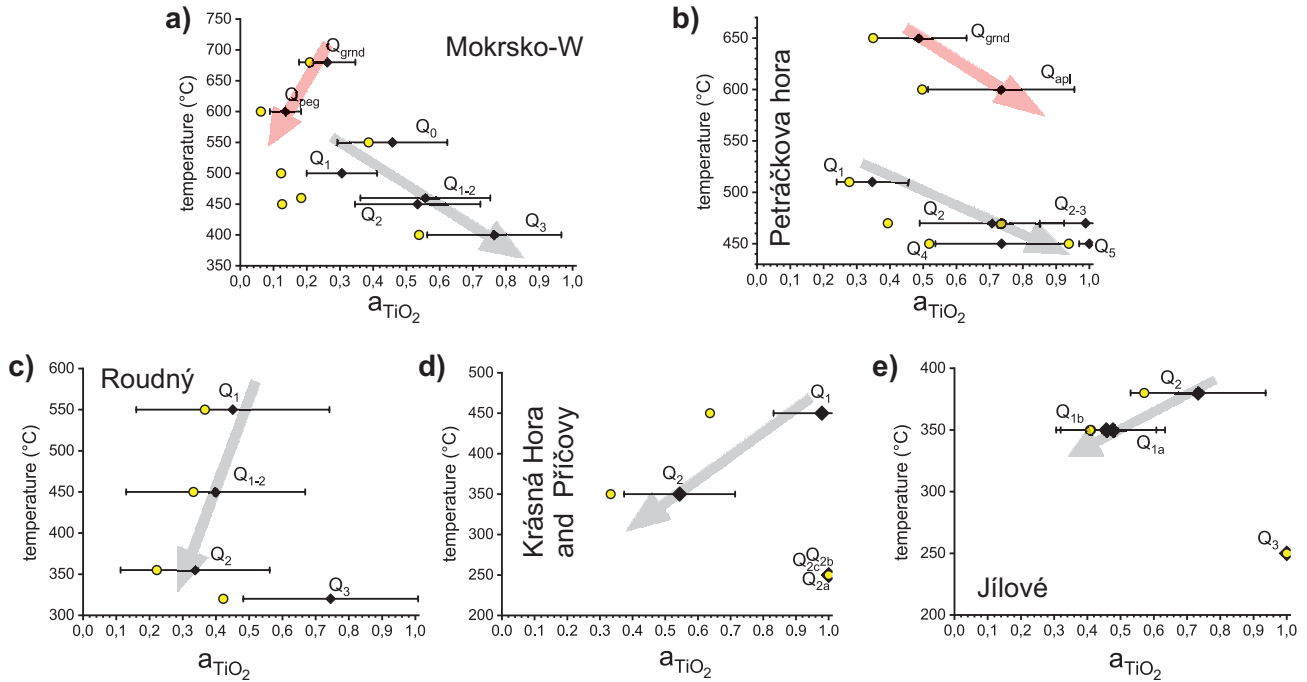


Fig. 5 Calculated a_{TiO_2} values, based on the calibration of Thomas et al. (2010), during quartz formation at the Mokrsko-West (a), Petrůčkova hora (b), Roudný (c), Krásná Hora and Příčovy (d), and Jílové (e) deposits. Black-filled diamond and open-circle (yellow) symbols differentiate among data based on median and minimum Ti abundances, respectively.

growth zones or grain clusters with substantially different CL-luminescence color and intensity were identified, but a few samples from the Krásná Hora Au-Sb deposit (Q_2) exhibited subtle sector zoning.

4.2. Overview of variations in Ti abundances

Figure 2a and Table 2 summarize the main descriptive statistic parameters of the measured Ti abundances individually for each quartz vein type. Titanium abundances approach right-skewed lognormal distribution in most quartz vein types (Fig. 2b). Variations in the measured Ti abundances, expressed as “median absolute deviation” (MAD) of the median, and the interquartile range (IQR) can be found in Table 2. The MAD and IQR values increase with both increasing pressure and increasing temperature.

4.3. Estimation of a_{TiO_2} using the Thomas et al. (2010) calibration

Figure 5 shows plots of a_{TiO_2} values based on the median and minimum Ti contents of the studied quartz samples, independently established P–T conditions and equation of Thomas et al. (2010). The error bars associated with the a_{TiO_2} values were calculated from the overall uncertainty in the P and T estimates, as $\pm 20\%$ of the P-value and as $\pm 5\%$ of the T value. For example, the uncertainty was set at ± 0.6 kbar and $\pm 15^\circ\text{C}$ for quartz formed at 3 kbar and 300°C . The data are plotted with respect to the quartz

formation temperature. Data without error bars plotted at $a_{TiO_2} = 1$ resulted in $a_{TiO_2} > 1$, theoretically not realistic (and may indicate kinetic effects or disequilibrium in general).

4.3.1. Mokrsko-West Au deposit

The calculated a_{TiO_2} values are lowest for the quartz of magmatic origin, representing the host granodiorite ($a_{TiO_2} = 0.26\text{--}0.21$; for median and minimum Ti abundance in Q_{gmd} , respectively) and a small pegmatite body ($a_{TiO_2} = 0.14\text{--}0.06$; Q_{peg}) at its exocontact. On the other hand, the a_{TiO_2} values of the ore-bearing hydrothermal veins (Q_1 to Q_3) increase gradually from 0.31 to 0.76. This trend reflects both decreasing age and temperature. The P–T conditions of the barren pre-ore Q_0 veins were arbitrarily set at 550°C and 4 kbar, as there is textural evidence for thermally driven solid-state recrystallization of the Q_0 quartz (i.e., contact metamorphism).

4.3.2. Petrůčkova hora Au deposit

Magmatic quartz (Q_{gmd}) of the host granodiorite yielded $a_{TiO_2} = 0.48\text{--}0.35$. Two other samples, associated with the same magmatic stage/event, resulted both in larger ($a_{TiO_2} = 0.73\text{--}0.50$; Q_{apl} ; quartz lens enclosed in an aplite dyke) and smaller ($a_{TiO_2} = 0.35\text{--}0.28$; Q_1 ; early quartz vein with high-temperature alteration rims) values. All the other quartz veins ($Q_2\text{--}Q_5$) yielded larger a_{TiO_2} values than the granodiorite (Q_{gmd}).

4.3.3. Roudný Ag–Au deposit

The a_{TiO_2} values of the barren pre-ore veins (Q_1) and ore-bearing veins (Q_{1-2} , Q_2) exhibit a slight decrease from 0.45–0.24 to 0.34–0.22 with decreasing temperature and towards late veins. If uncertainty associated with a_{TiO_2} estimation is included, then the a_{TiO_2} values of all the above-mentioned vein types are statistically indistinguishable. Late quartz (Q_3), however, has an a_{TiO_2} value that is about twice as large ($a_{TiO_2} = 0.75–0.42$).

4.3.4. Krásná Hora and Příčovy Sb–Au deposits

Pre-ore barren veins (Q_1) at the Krásná Hora deposit have an $a_{TiO_2} = 0.98–0.64$. All kinds of the ore-bearing quartz (Q_{2a} , Q_{2b} , Q_{2c}) of the Příčovy deposit suggest disequilibrium Ti content. On the other hand, Q_2 quartz of the main-ore-stage at Krásná Hora exhibits intermediate values ($a_{TiO_2} = 0.54–0.33$).

4.3.5. Jílové Au deposit

The most abundant vein quartz (Q_1) yielded a_{TiO_2} values between ~ 0.4 and ~ 0.5 . Unusual, molybdenite-bearing quartz (Q_2) sample had a larger a_{TiO_2} value (0.73–0.57). The latest (i.e., youngest) quartz (Q_3), associated with deposition of native arsenic, indicates disequilibrium conditions. The relative chronology of the molybdenite-bearing quartz vein with respect to the other vein types is uncertain (i.e., Q_2 may be older or younger than Q_1).

5. Discussion

5.1. Sensitivity of Ti-in-quartz thermobarometry to changes in P, T, a_{TiO_2}

Figure 6 summarizes the relative changes in Ti abundances of the quartz (calculated after Thomas et al. 2010) to moderate changes in the pressure, temperature and a_{TiO_2} :

The results are expressed as the relative percentages of the initial Ti content (representing 100 %) of the previous calculation step (the calculation steps were equal to 0.1 a_{TiO_2} in Fig. 6a or to 25 °C in Figs. 6b–c). First, the absolute Ti abundances were calculated for all the possible combinations of T (200–900 °C, step 25 °C), P (1–8 kbar, step 0.25 kbar) and a_{TiO_2} (0.05–1.0, step 0.05). Then the relative changes (rel. %) in the Ti abundances were calculated by comparing the data representing conditions when two variables stayed fixed (e.g., P, T), while the third variable could vary as indicated in the label box for each figure.

For an initial value of a_{TiO_2} in the range 1.0 to 0.5, a decrease in a_{TiO_2} by a value of 0.1 leads to a reduction in the Ti concentration to 90–80 % of its original value (Fig. 6a). If the initial value of a_{TiO_2} is smaller than 0.5, then the relative decrease in Ti is larger (Fig. 6a). In contrast, a decrease in pressure at constant temperature and constant a_{TiO_2} leads to an increase in the Ti content. A pressure decrease of 1 kbar increases the Ti content to up to 120 % of its initial value at the high-temperature settings and up to 140 % at low-temperature settings. A decrease in temperature, at constant pressure and constant a_{TiO_2} , leads to a decrease in the Ti content. For example, a temperature decrease by 10 °C results in a decrease in the Ti content to 90–70 % of the original value, with the exact value depending on the initial temperature (Fig. 6c). Minor to moderate variations in P, T and a_{TiO_2} can thus easily fully or partly contribute to the observed range of Ti abundances in a single quartz vein sample.

The Figure 7 documents the variability of the measured Ti abundances expressed as the relative difference between the minimum or maximum values and the mean Ti value for a given vein type (using the median instead of mean values does not substantially affect the plot). We can see that the relative differences tend to increase towards lower temperatures and pressures. The trend of natural data (Fig. 7) is thus similar to that of the theoretical ones (Fig. 6b–c).

The Ti abundances for individual quartz vein types tend to approach lognormal distribution skewed toward

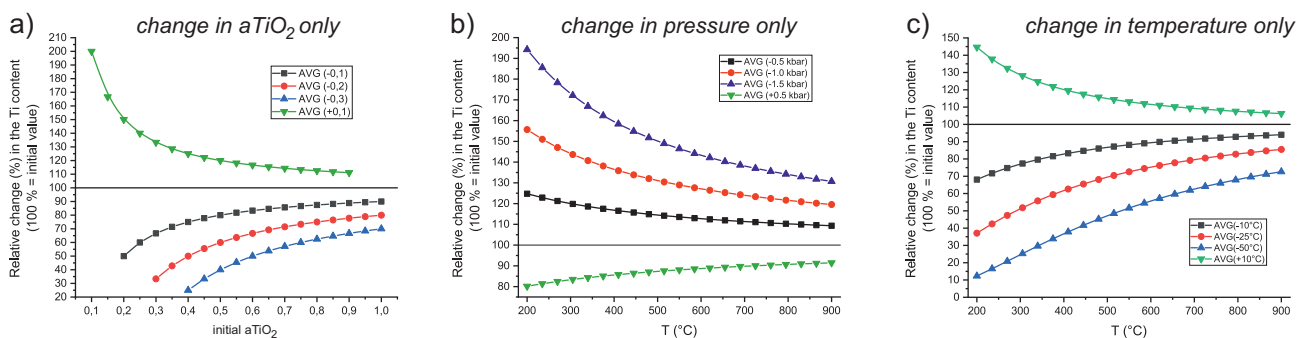


Fig. 6 Relative changes in the initial Ti abundance (expressed as 100 %) with moderate changes in the a_{TiO_2} (a), pressure (b) and temperature (c). All the calculations are based on the Thomas et al. (2010) relationship between the Ti abundance and P, T and a_{TiO_2} .

higher concentration (Fig. 2b herein, or Fig. 2 in Pacák et al. 2019). This is in line with the exponential effect of temperature on Ti concentration. However, if the quartz crystallized in a normal distribution around the median temperature (in temperature space), a skew right distribution of Ti abundances is the result. This suggests that intra-vein variations in the quartz crystallization temperature are probably the main cause of observed variations in Ti abundances. In the end, larger relative uncertainties in measured Ti also likely play a role in increasing (relative) scatter of data at low Ti concentrations (and low T).

5.2. Apparent disequilibrium due to kinetics effects

Another possible source of Ti-abundance variations on the sample scale is quartz disequilibrium formation due to a variable/faster growth rate. Huang and Audétat (2012) identified up to about 2.5 times greater Ti abundance in rapidly grown quartz ($\sim 110 \mu\text{m}/\text{day}$) compared to a slowly grown sample ($\sim 4 \mu\text{m}/\text{day}$). Therefore, they used the Ti concentration of the most slowly grown quartz samples for calibration of their thermobarometry. Acosta et al. (2020) give a more in-depth discussion of various kinetic effects. These are, however, difficult to employ in the study of natural samples.

In order to quantify the apparent degree of disequilibrium, we propose following relationship:

$$X^* = \frac{T_{i_{\text{measured}}}}{T_{i_{\text{eq}}}} \quad (1)$$

where $T_{i_{\text{measured}}}$ refers to the measured Ti concentration in a quartz sample (we used the median value of measured Ti concentration as a representative value for each vein-type), while $T_{i_{\text{eq}}}$ refers to “the equilibrium” Ti content in quartz calculated using the corresponding thermobarometer – $X^*(\text{TH10})$ – Thomas et al. (2010) – for a given P–T and assuming $a_{\text{TiO}_2} = 1$.

For example, the application of the calibration of Thomas et al. (2010) predicts 32.34 ppm Ti ($a_{\text{TiO}_2} = 1.0$), or 16.17 ppm Ti ($a_{\text{TiO}_2} = 0.5$) for quartz formed at 500 °C and 3 kbar. Let us consider a natural sample formed at 500 °C and 3 kbar, however at unknown a_{TiO_2} . If the sample contains 32.34 ppm Ti, value $X^*(\text{TH10}) = 1$ (i.e., 32.24/32.34), if the Ti content is lower, e.g., 16.17 ppm, then value $X^*(\text{TH10}) = 0.5$ (i.e., 16.17/32.34). On the other hand, 50 ppm Ti results in $X^*(\text{TH10}) = 1.55$ (i.e., 50/32.34). The latter content (50 ppm) is higher than the maximum solubility of Ti in quartz for a given P–T after the model of Thomas et al. (2010) and is therefore theoretically unrealistic. Value $X^* = 1$ implies that the quartz grew at $a_{\text{TiO}_2} = 1$ in equilibrium with the model. Note that

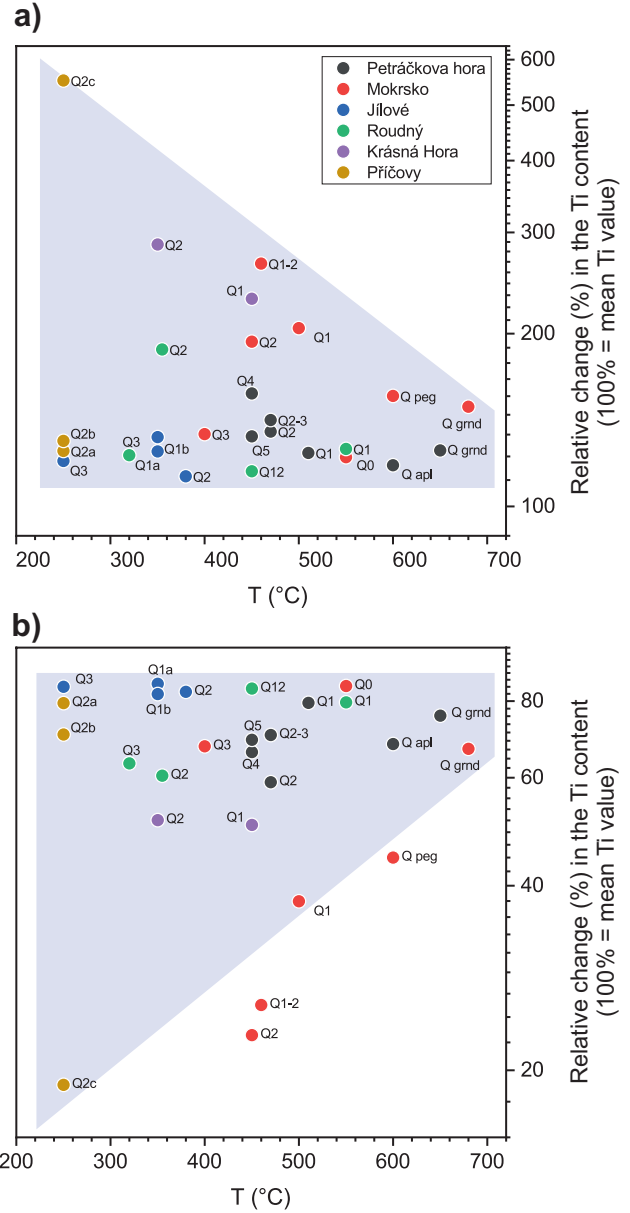


Fig. 7 The measured maximum (a) and minimum (b) Ti abundances are expressed as their relative difference to the mean values (mean = 100 %). The magnitude of the relative differences tends to increase with decreasing temperature, schematically highlighted by the shaded area.

for $X^* \leq 1$, the X^* values are identical with the estimation of a_{TiO_2} following the model, while $X^* > 1$ implies oversaturation of the quartz with respect to rutile (for a given P–T) and represents a measure of the relative Ti disequilibrium enrichment compared to the model (Thomas et al. 2010 in our case).

Figure 8 summarizes the $X^*(\text{TH10})$ data for all the studied quartz vein types taken from selected Bohemian gold deposits. The value $X^* = 1$ is highlighted by a red dashed line. Data plotted to the left of the red line

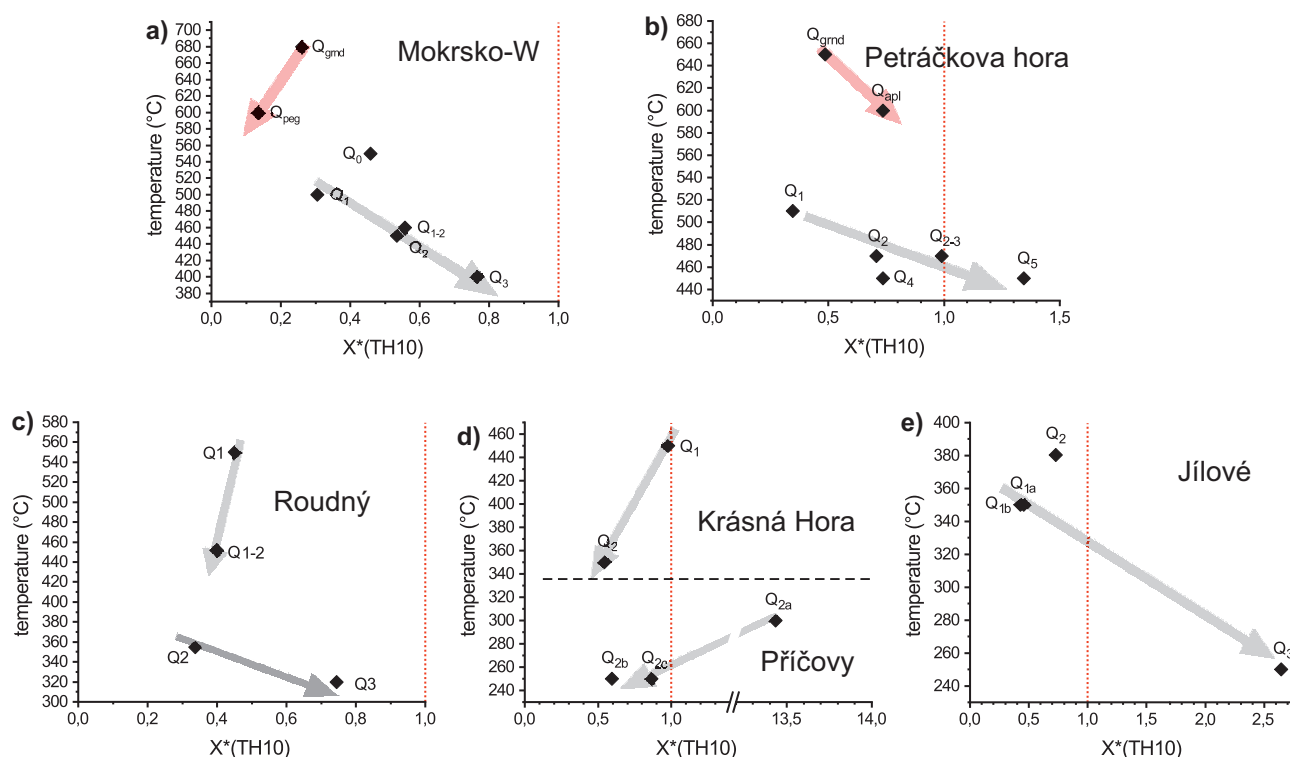


Fig. 8 Apparent measure of equilibrium/disequilibrium Ti content (see the discussion for the definition of X^*) in quartz samples from various gold deposits: **a** – Mokrsko-West (IRG); and **b** – Petráčková hora (IRG); **c** – Roudný (ORG); **d** – Krásná Hora (ORG Sb–Au) and Příčovy (ORG Sb–Au); and **e** – Jílové (ORG). Values $X^* > 1$ imply disequilibrium quartz formation, values $X^* \leq 1$ correspond to the hypothetical maximum a_{TiO_2} value for the given quartz type (suggesting that calibration of Thomas et al. (2010) represents equilibrium Ti contents).

($X^* = 1$) thus correspond to maximum a_{TiO_2} for a given vein type, while those plotted to the right ($X^* > 1$) indicate apparent Ti-oversaturation. Most of our data exhibit $X^* \leq 1$, notably those for the IRG deposits (Mokrsko and Petráčková hora).

There is a general tendency towards a gradual increase in X^* values as the quartz formation temperature (and pressure) decrease(s). This is clearly discernible for both IRG deposits (Mokrsko and Petráčková hora) and certain ORG deposits (Jílové). The anomalous “behavior” of the Q_1 data from the Roudný ORG deposit (Fig. 8c) may be related to the formation of these veins from genetically distinct metamorphic fluids. A single quartz type/sample – Q_{2a} – quartz from the Příčovy Sb–Au deposit – deviates substantially from the other data, exhibiting much higher X^* values, ranging from 13.4 at 300 °C (Fig. 8d) to ~47 at 250 °C. It differs substantially from the X^* values of veins Q_{2b} ($X^* = 0.9$ to 2.1) and Q_{2c} ($X^* = 0.9$ to 3.0) from the same deposit calculated for the same temperature range (Fig. 8d). Note also that Q_{2a} and Q_{2b} quartz types occur together in a single vein/sample (Fig. 4d). The quartz grain size is the main difference between the Q_{2a} and Q_{2b} – Q_{2c} quartz types. The Q_{2a} quartz, although α -quartz, is extremely fine-grained (median 30 μm ; Fig. 4a), compared to the Q_{2b} (median 200 μm ; Fig. 4b), and Q_{2c} (median 147 μm ; Figs 4c and 4e) samples. They are all

intergrown with Sb-bearing phases, thus confirming affiliation to the same paragenetic stage and consequently formation under the same/similar P–T conditions. These are estimated to be at least about 250 °C and 1–0.6 kbar, based on homogenization temperatures of primary fluid inclusions in Q_{2b} (195 ± 21 °C; see Figs 11 and 14 in Němec and Zachariáš 2018).

This all demonstrates that parameter X^* is an appropriate measure of quartz disequilibrium formation relative to the used experimental or thermodynamic model. The much higher Ti content (20 to 31 ppm Ti) of the extremely fine-grained Q_{2a} quartz, compared to the more coarse-grained Q_{2b} and Q_{2c} quartz (~1 to ~4 ppm Ti), can be best explained by its sudden grain nucleation, faster growth rate and precipitation from a supersaturated solution. This resulted in its chalcedony-like appearance, although it is α -quartz. We are unaware of such extreme Ti enrichment ($19\times$ to $28\times$; based on the ratio of median Ti abundances) in quartz because of its rapid growth rate.

5.3. Quartz formation under open and closed system conditions

Two patterns seem to reflect a_{TiO_2} evolution trends among the studied deposits. These patterns can be recognized on both the a_{TiO_2} – T (Fig. 5) and X^* – T plots (Fig. 8). The

patterns seem to reflect mainly decreasing temperature during vein formation and, to a lesser extent, also the genetic type of a gold deposit (IRG vs. ORG).

The Petráčková hora and Mokrsko-West deposits can be considered to be the most typical representatives of IRG deposits in the Bohemian Massif. They indicate spatial and temporal relationships to a magmatic body/suite, the high-temperature nature of early fluids/veins, a large abundance of the Bi–(Te) phases and the absence of wide-spread intense hydrothermal alteration. The values of a_{TiO_2} and X^* of the vein quartz of IRG deposits systematically increase over time as the parent fluid cools. The latest (i.e., youngest) quartz veins exhibit the largest a_{TiO_2} or X^* values. This suggests apparent saturation of the fluid with respect to rutile, most likely due to a decrease in the solubility of rutile at lower temperatures (Antignano and Manning 2008). The trend can be interpreted as quartz vein formation under closed-system conditions (i.e., without equilibration between the fluid and the surrounding rocks). This suggestion is further supported by the high variability of the calculated a_{TiO_2} or X^* values, in spite of vein quartz precipitation within a geochemically and mineralogically “homogeneous” granodiorite body.

The evolutionary pattern of the a_{TiO_2} or X^* values of the ORG deposits is less obvious. The data display a slight gradual decrease in a_{TiO_2} or X^* values, along with decreasing temperature of the vein formation. This trend is difficult to assign to either open or closed system behavior because it is probable that these veins were formed from more than a single fluid source. The difference in a_{TiO_2} or X^* patterns, between the IRG and ORG deposits, is, however, evident.

6. Conclusions

The titanium content of quartz vein samples from five Variscan Bohemian gold deposits with known P–T history were used to calculate the titanium oxide activities (a_{TiO_2}) of hydrothermal quartz grown naturally in the absence of a_{TiO_2} buffering phases at 250–550 °C and 0.1–4 kbar. Variations in Ti abundances in the studied quartz reflect variations in all the potential variables (P, T, a_{TiO_2} and quartz growth rate). Despite this complexity, our calculations also support significant variations in a_{TiO_2} during the vein formation. In addition, we found evidence for the formation of quartz veins at intrusion-related gold deposits under closed-system conditions. This suggests the absence/minimum of fluid equilibration with the host rocks along the fluid ascending path. Most of our data are consistent with the Thomas et al. (2010) solubility model and suggest quartz formation in a systematically undersaturated system with respect to rutile. Finally, we proposed a new formula for quantifying the degree of

quartz disequilibrium precipitation regarding Ti abundance in quartz. The formula was successfully applied to a natural quartz sample showing textural and grain-size evidence of rapid non-equilibrium crystallization.

Acknowledgments: This research was supported by the Grant Agency of Charles University (project GAUK 392715). Finalization of the manuscript benefited from the financial support of the Cooperatio Program, GEOL section. Also, we would like to thank M. Štulíková for editing the English language manuscript. Furthermore, the present version benefitted from the constructive comments of M. R. Ackerson and an anonymous reviewer. We also appreciate the comments of the handling editor J. Hora.

Electronic supplementary material. A brief description of the studied deposits is available online at the Journal web site (<http://dx.doi.org/10.3190/jgeosci.340>).

References

- Ackerman L, Haluzová E, Creaser RA, Pašava J, Veselovský F, Breiter K, Erban V, Drábek M (2017) Temporal evolution of mineralization events in the Bohemian Massif inferred from the Re–Os geochronology of molybdenite. *Miner Depos* 52: 651–662
- ACKERSON MR, MYSEN BO, TAILBY ND, WATSON EB (2018) Low-temperature crystallization of granites and the implications for crustal magmatism. *Nature* 559: 94–97
- ACOSTA MD, WATKINS JM, REED MH, DONOVAN JJ, DE-PAOLO DJ (2020) Ti-in-quartz: Evaluating the role of kinetics in high temperature crystal growth experiments. *Geochim Cosmochim Acta* 281: 149–167
- ALLAN MM, YARDLEY BWD (2007) Tracking meteoric infiltration into a magmatic-hydrothermal system: A cathodoluminescence, oxygen isotope and trace element study of quartz from Mt. Leysdon, Australia. *Chem Geol* 240: 343–360
- ANTIGNANO A, MANNING CE (2008) Rutile solubility in H_2O , H_2O – SiO_2 , and H_2O – $\text{NaAlSi}_3\text{O}_8$ fluids at 0.7–2.0 GPa and 700–1000 °C: Implications for mobility of nominally insoluble elements. *Chem Geol* 255: 283–293
- ASHLEY KT, LAW RD (2015) Modeling prograde TiO_2 activity and its significance for Ti-in-quartz thermobarometry of pelitic metamorphic rocks. *Contrib Mineral Petrol* 169: 1–7
- ASHLEY KT, WEBB LE, SPEAR FS, THOMAS JB (2013) P–T–D histories from quartz: A case study of the application of the TitaniQ thermobarometer to progressive fabric development in metapelites. *Geochem Geophys Geosyst* 14: 3821–3843
- BARKER AK, COOGAN LA, GILLIS KM, HAYMAN NW, WEIS D (2010) Direct observation of a fossil high-temperature,

- fault-hosted, hydrothermal upflow zone in crust formed at the East Pacific Rise. *Geology* 38: 379–382
- BESTMANN M, PENNACCHIONI G, MOSTEFAOUI S, GÖKEN M, DE WALL H (2016) Instantaneous healing of microfractures during coseismic slip: Evidence from microstructure and Ti in quartz geochemistry within an exhumed pseudotachylyte-bearing fault in tonalite. *Lithos* 254–255: 84–93
- BOIRON MC, BARAKAT A, CATHELINÉAU M, BANKS DA, DURISOVA J, MORAVEK P (2001) Geometry and P–V–T–X conditions of microfissural ore fluid migration: the Mokrsko gold deposit (Bohemia). *Chem Geol* 173: 207–225
- BREITER K, SVOJTKA M, ACKERMAN L, ŠVECŮVÁ K (2012) Trace element composition of quartz from the Variscan Altenberg–Teplice caldera (Krušné hory/Erzgebirge Mts, Czech Republic/Germany): Insights into the volcano-plutonic complex evolution. *Chem Geol* 326–327: 36–50
- BUTHELEZI M, ASHWAL LD, HORVÁTH P (2017) Application of titanium-in-quartz geothermometry to magmatic quartz in evolved rocks from the Bushveld Complex, South Africa. *S Afr J Geol* 120: 241–250
- CAVALCANTE GCG, VAUCHEZ A, MERLET C, EGYDIO-SILVA M, DE HOLANDA MHB, BOYER B (2014) Thermal conditions during deformation of partially molten crust from TitaniQ geothermometry: Rheological implications for the anatexis domain of the Araçuaí belt, eastern Brazil. *Solid Earth* 5: 1223–1242
- CERNUSCHI F, DILLES JH, GROCKE SB, VALLEY JW, KITAJIMA K, TEPLY FJ (2018) Rapid formation of porphyry copper deposits evidenced by diffusion of oxygen and titanium in quartz. *Geology* 46: 611–614
- CRUZ-URIBE AM, MERTZ-KRAUS R, ZACK T, FEINEMAN MD, WOODS G, JACOB DE (2017) A New LA-ICP-MS method for Ti in Quartz: Implications and application to high pressure rutile-quartz veins from the Czech Erzgebirge. *Geostand Geoanal Res* 41: 29–40
- DALLMEYER RD, FRANKE W, WEBER K (eds) (1995) *Pre-Permian Geology of Central and Eastern Europe*. Springer-Verlag, Berlin, pp 1–593
- EHRlich K, VERŠ E, KIRS J, SOESOO A (2012) Using a titanium-in-quartz geothermometer for crystallization temperature estimation of the Palaeoproterozoic Suurvaari quartz porphyry. *Est J Earth Sci* 61: 195–204
- GRUJIC D, STIPP M, WOODEN JL (2011) Thermometry of quartz mylonites: Importance of dynamic recrystallization on Ti-in-quartz reequilibration. *Geochem Geophys Geosyst* 12, Q06012
- HAERTEL M, HERWEGH M, PETTKE T (2013) Titanium-in-quartz thermometry on synkinematic quartz veins in a retrograde crustal-scale normal fault zone. *Tectonophysics* 608: 468–481
- HAJNÁ J, ŽÁK J, KACHLÍK V (2011) Structure and stratigraphy of the Teplá–Barrandian Neoproterozoic, Bohemian Massif: a new plate-tectonic reinterpretation. *Gondwana Res* 19: 495–508
- HOLUB F, MACHART J, MANOVÁ M (1997) The Central Bohemian Plutonic Complex Geology, chemical composition and genetic interpretation. *Sbor Geol Věd, Ložisk geol-mineral (Praha)* 31, 27–50
- HUANG R, AUDÉTAT A (2012) The titanium-in-quartz (TitaniQ) thermobarometer: A critical examination and re-calibration. *Geochim Cosmochim Acta* 84: 75–89
- JANOŠEK V, GERDES A (2003) Timing the magmatic activity within the Central Bohemian Pluton, Czech Republic: conventional U–Pb ages for the Sázava and Tábora intrusions and their geotectonic significance. *J Czech Geol Soc* 48: 70–71
- JANOŠEK V, BRAITHWAITE CJR, BOWES DR, GERDES A (2004) Magma-mixing in the genesis of Hercynian calc-alkaline granitoids: an integrated petrographic and geochemical study of the Sázava intrusion, Central Bohemian Pluton, Czech Republic. *Lithos* 78: 67–99
- JANOŠEK V, WIEGAND BA, ŽÁK J (2010) Dating the onset of Variscan crustal exhumation in the core of the Bohemian Massif: new U–Pb single zircon ages from the high-K calc-alkaline granodiorites of the Blatná suite, Central Bohemian Plutonic Complex. *J Geol Soc* 167: 347–360
- KENDRICK J, INDARES A (2018) The Ti Record of Quartz in Anatexis Aluminous Granulites. *J Petrol* 59: 1493–1516
- KIDDER SB, TOY VG, PRIOR DJ, LITTLE TA, KHAN A, MACRAE C (2018) Constraints on Alpine Fault (New Zealand) mylonitization temperatures and the geothermal gradient from Ti-in-quartz thermobarometry. *Solid Earth* 9: 123–1139
- KOHN MJ, NORTHRUP CJ (2009) Taking mylonites' temperatures. *Geology* 37: 47–50
- LINNEMANN U, PEREIRA F, JEFFRIES TE, DROST K, GERDES A (2008) The Cadomian Orogeny and the opening of the Rheic Ocean: the diachrony of geotectonic processes constrained by LA-ICP-MS U–Pb zircon dating (Ossa-Morena and Saxo-Thuringian zones, Iberian and Bohemian massifs). *Tectonophysics* 461: 21–43
- MONNIER L, LACH P, SALVI S, MELLETON J, BAILLY L, BÉZIAT D, MONNIER Y, GOUY S (2018) Quartz trace-element composition by LA-ICP-MS as proxy for granite differentiation, hydrothermal episodes, and related mineralization: The Beauvoir Granite (Echassières district), France. *Lithos* 320–321: 355–377
- MORÁVEK P (1971) Ore-deposits structure and mineralization of the Jílové gold-mining district (in Czech with extensive English summary). *Sb geol Věd, řada LG* 13, 1–170
- MORÁVEK P, JANATKA J, PERTOLDOVÁ J, STRAKA E, ĎURIŠOVÁ J, PUDILOVÁ M (1989) Mokrsko gold deposit – the largest gold deposit in the Bohemian Massif, Czechoslovakia. *Econ Geol Monograph* 6: 252–259

- MORGAN DJ, JOLLANDS MC, LLOYD GE, BANKS DA (2014) Using titanium-in-quartz geothermometry and geospeedometry to recover temperatures in the aureole of the Ballachulish Igneous Complex, NW Scotland. *Geol Soc, London, Spec Publ* 394, 145–165
- MÜLLER A, IHLEN PM, WANVIK JE, FLEM B (2007) High-purity quartz mineralisation in kyanite quartzites, Norway. *Miner Depos* 42: 523–535 (2008) Compositional zoning of rapakivi feldspars and coexisting quartz phenocrysts. *Canad Mineral* 46: 1417–1442
- MÜLLER A, WANVIK JE, IHLEN PM (2012) Petrological and chemical characterisation of high-purity quartz deposits with examples from Norway. In GÖTZE J, MÖCKEL R (eds) *Quartz: Deposits, mineralogy and analytics*. Springer, Berlin, Heidelberg, p 71–118
- NACHLAS WO, HIRTH G (2015) Experimental constraints on the role of dynamic recrystallization on resetting the Ti-in-quartz thermobarometer. *J Geophys Res: Solid Earth* 120: 8120–8137
- NACHLAS WO, WHITNEY DL, TEYSSIER C, BAGLEY B, MULCH A (2014) Titanium concentration in quartz as a record of multiple deformation mechanisms in an extensional shear zone. *Geochem Geophys Geosyst* 15: 1374–1397
- NACHLAS WO, THOMAS JB, HIRTH G (2018) TitaniQ deformed: Experimental deformation of out-of-equilibrium quartz porphyroclasts. *J Struct Geol* 116: 207–222
- NEGRINI M, STUNITZ H, BERGER A, MORALES LFG (2014) The effect of deformation on the TitaniQ geothermobarometer: An experimental study. *Contrib Mineral Petrol* 167: 1–22
- NĚMEC M, ZACHARIÁŠ J (2018) The Krásná Hora, Milešov, and Příčovy Sb–Au ore deposits, Bohemian Massif: mineralogy, fluid inclusions, and stable isotope constraints on the deposit formation. *Miner Depos* 53: 225–244
- NEVITT JM, WARREN JM, KIDDER S, POLLARD DD (2017) Comparison of thermal modeling, microstructural analysis, and Ti-in-quartz thermobarometry to constrain the thermal history of a cooling pluton during deformation in the Mount Abbot Quadrangle, CA. *Geochem Geophys Geosyst* 18: 1270–1297
- O'BRIEN PJ (2000) The fundamental Variscan problem: high-temperature metamorphism at different depths and high-pressure metamorphism at different temperatures. In: Franke W, Haak V, Oncken O, Tanner D (eds) *Orogenic Processes: Quantification and Modelling in the Variscan Belt*. Geol Soc, London, Spec Publ 179, 369–386
- O'BRIEN PJ, RÖTZLER J (2003) High-pressure granulites: formation, recovery of peak conditions and implications for tectonics. *J Metamorph Geol* 21: 3–20
- OSTAPENKO GT, BAMARNIK MY, GOROGOTSKAYA LI (1987) Isomorphism of titanium substitution for silicon in quartz: experimental data. *Mineral Zh* 9: 30–40
- PACÁK K, ZACHARIÁŠ J, STRNAD L (2019) Trace-element chemistry of barren and ore-bearing quartz of selected Au, Au–Ag and Sb–Au deposits from the Bohemian Massif. *J Geosci* 64: 19–35
- PÉREZ-ALONSO J, FERTES-FUENTE M, BASTIDA F (2016) Quartz veining in slates and Variscan deformation: Insights from the Lúcar sector (NW Spain). *Tectonophysics* 671: 24–41
- RUSK BG, LOWERS HA, REED MH (2008) Trace elements in hydrothermal quartz: Relationships to cathodoluminescent textures and insights into vein formation. *Geology* 36: 547–550
- RUSK B, KOENIG A, LOWERS H (2011) Visualizing trace element distribution in quartz using cathodoluminescence, electron microprobe, and laser ablation-inductively coupled plasma-mass spectrometry. *Amer Miner* 96: 703–708
- SCHULMANN K, KONOPÁSEK J, JANOUŠEK V, LEXA O, LARDEAUX JM, EDEL JB, ŠTIPSKÁ P, ULRYCH S (2009) An Andean type Palaeozoic convergence in the Bohemian Massif. *C R Geosci* 341: 266–286
- SIMON K, SCHERER T, VAN DEN KERKHOF AM, KRONZ A (2004) Fluid-controlled quartz recovery in granulite as revealed by cathodoluminescence and trace element analysis (Bamble sector, Norway). *Contrib Mineral Petrol* 146: 637–652
- SPEAR FS, WARK DA (2009) Cathodoluminescence imaging and titanium thermometry in metamorphic quartz. *J Metamorph Geol* 27, 187–205
- STORM LC, SPEAR FS (2009) Application of the titanium-in-quartz thermometer to pelitic migmatites from the Adirondack Highlands, New York. *J Metamorph Geol* 27: 479–494
- THOMAS JB, WATSON EB, SPEAR FS, SHEMELLA PT, NAYAK SK, LANZIROTTI A (2010) TitaniQ under pressure: The effect of pressure and temperature on the solubility of Ti in quartz. *Contrib Mineral Petrol* 160: 743–759
- THOMAS JB, WATSON EB, SPEAR FS, WARK DA (2015) TitaniQ recrystallized: experimental confirmation of the original Ti-in-quartz calibrations. *Contrib Mineral Petrol* 169: 27
- VAN DEN KERKHOF AM, KRONZ A, SIMON K, RIGANTI A, SCHERER T (2004) Origin and evolution of Archean quartzites from the Nondweni greenstone belt (South Africa): inferences from a multidisciplinary study. *S Afr J Geol* 107: 559–576
- WARK DA, WATSON EB (2006) TitaniQ: A titanium-in-quartz geothermometer. *Contrib Mineral Petrol* 152: 743–754
- WERTICH V, LEICHMANN J, DOSBABA M, GÖTZE J (2018) Multi-Stage Evolution of Gold-Bearing Hydrothermal Quartz Veins at the Mokrsko Gold Deposit (Czech Republic) Based on Cathodoluminescence, Spectroscopic, and Trace Elements Analyses. *Minerals* 8: 335
- WIEBE RA, WARK DA, HAWKINS DP (2007) Insights from quartz cathodoluminescence zoning into crystallization of the Vinalhaven granite, coastal Maine. *Contrib Mineral Petrol* 154: 439–453

- ZACHARIÁŠ J (2016) Structural evolution of the Mokrsko-West, Mokrsko-East and Čelina gold deposits, Bohemian Massif, Czech Republic: Role of fluid overpressure. *Ore Geol Rev* 74: 170–195
- ZACHARIÁŠ J, HÜBST Z (2012) Structural evolution of the Roudný gold deposit. Bohemian Massif: A combination of paleostress analysis and review of historical documents. *J Geosci* 57: 87–103
- ZACHARIÁŠ J, NĚMEC M (2017) Gold to aurostibite transformation and formation of Au–Ag–Sb phases: the Krásná Hora deposit, Czech Republic. *Mineral Mag* 81: 987–999
- ZACHARIÁŠ J, STEIN H (2001) Re–Os ages of Variscan hydrothermal gold mineralizations, Central Bohemian metallogenic zone. In PIĘSTRZYŃSKI et al. (eds) *Mineral Deposits at the Beginning of the 21st Century*. Swets & Zeitlinger Publishers Lisse, pp 851–854
- ZACHARIÁŠ J, PERTOLD Z, PUDILOVÁ M, ŽÁK K, PERTOLDOVÁ J, STEIN H, MARKEY R (2001) Geology and genesis of Variscan porphyry-style gold mineralization, Petráčková hora deposit, Bohemian Massif, Czech Republic. *Miner Depos* 36: 517–541
- ZACHARIÁŠ J, FRÝDA J, PATEROVÁ B, MIHALJEVIČ M (2004) Arsenopyrite and As-bearing pyrite from the Roudný deposit, Bohemian Massif. *Mineral Mag* 68: 31–46
- ZACHARIÁŠ J, PATEROVÁ B, PUDILOVÁ M (2009) Mineralogy, fluid Inclusion, and stable isotope constraints on the genesis of the Roudný Au–Ag deposit, Bohemian Massif. *Econ Geol* 104: 53–72
- ZACHARIÁŠ J, ŽÁK K, PUDILOVÁ M, SNEE LW (2013) Multiple fluid sources/pathways and severe thermal gradients during formation of the Jílové orogenic gold deposit, Bohemian Massif, Czech Republic. *Ore Geol Rev* 54: 81–109
- ZACHARIÁŠ J, MORÁVEK P, GADAS P, PERTOLDOVÁ J (2014) The Mokrsko-West gold deposit, Bohemian Massif, Czech Republic: mineralogy, deposit setting and classification. *Ore Geol Rev* 58: 238–263
- ZHANG CLX, ALMEEV RR, HORN I, BEHRENS H, HOLTZ F (2020) Ti-in-quartz thermobarometry and TiO₂ solubility in rhyolitic melts: New experiments and parametrization. *Earth Planet Sci Lett* 538: 116213